ORIGINAL PAPER

Separation of a heavy metal from water through a membrane containing boron nitride nanotubes: molecular dynamics simulations

Jafar Azamat · Alireza Khataee · Sang Woo Joo

Abstract Molecular dynamics simulations were performed to investigate the separation of zinc ions as a heavy metal from water using boron nitride nanotubes. The studied systems included boron nitride (BN) nanotubes embedded in a silicon-nitride membrane immersed in an aqueous solution of $ZnCl_2$. An external electric field was applied to the system along the axis of the BN nanotubes. The results show that the (7,7) and (8,8) BN nanotubes were exclusively selective of ions. The (7,7) BN nanotube selectively conducted Zn^{2+} ions, while the (8,8) BN nanotube selectively conducted Cl^- ions. The results were confirmed using additional simulated parameters. The results indicate that the passage of ions through nanotubes is related to the diameter of the BN nanotubes.

Keywords Boron nitride nanotube · Desalination · Heavy metals · Molecular dynamics · Nanostructured membrane

Introduction

The expansion of effective low-cost water desalination and methods for the removal of heavy metal ions such as zinc from water are important from both the environmental and economic perspectives. While organisms need heavy metals to perform their biological tasks, the toxic effect of these metals can contribute to neuronal disease pathogenesis. Although living organisms require low amounts of heavy metals, excessive amounts can be damaging. Toxicity from heavy metals can result in damaged or reduced mental and central nervous function. Therefore, the removal of heavy metal ions from contaminated water has become an important subject [1–8]. Zinc, a heavy metal, is necessary to humans because it contributes to the physiology of living tissue and biochemical processes. Nevertheless, high levels of zinc can cause human health disorders, such as stomach cramps, skin irritation, and vomiting [9]. Several techniques have been proposed for the elimination of heavy metals from wastewater, including ion-exchange [10], coagulation and flocculation [11], chemical precipitation [12], reverse osmosis [13], adsorption [14], and other methods [15–18].

Selective ion transport via nanostructures is of interest in a wide range of chemical and physical fields. Nanotubes have potential uses in the purification and desalination industries. Boron nitride (BN) nanotubes are important to researchers because of their significant electronic properties and structural uses [19–21]. In the field of fluid transport properties of the BN nanotubes, Aluru and coworkers reported the ionic selectivity of BN nanotubes relative to chloride and potassium ions and they showed that (10,10) BN nanotube could be transported by chloride ions [22]. Chen and coworkers have demonstrated that BN nanotubes had interactions with proteins and cells and their properties are encouraging for their application in biocompatible materials [23]. In other work, the structure and dynamics of water confined in BN nanotubes have been studied by MD method and the passage way of water molecules is investigated [24].

BN nanotubes have chirality, which is a geometrical parameter; however, in terms of controlling electrical properties, chirality does not play a significant role [25]. BN nanotube was theoretically predicted in 1994 [26] and then

J. Azamat · A. Khataee (✉)
Research Laboratory of Advanced Water and Wastewater Treatment Processes, Department of Applied Chemistry, Faculty of Chemistry, University of Tabriz, 51666-14766 Tabriz, Iran
e-mail: a_khataee@tabrizu.ac.ir

A. Khataee
e-mail: ar_khataee@yahoo.com

S. W. Joo (✉)
School of Mechanical Engineering, Yeungnam University, Gyeongsan 712-749, South Korea
e-mail: swjoo@yu.ac.kr

experimentally synthesized in 1995 [27]. In recent years, most studies have been done on the synthesis of BN nanotubes [28–31]. To date, scientists designed and synthesized ion-selective nanotubes [22, 32–35].

Due to the lack of theoretical studies on zinc ion separation from water through a membrane containing BN nanotubes, here we apply molecular dynamics simulation techniques and investigate the removal of zinc from aqueous solutions using BN nanotubes. We used BN nanotubes with (7,7) and (8,8) chirality, fixed in a silicon-nitride membrane, and immersed in 0.5 mol L^{-1} ZnCl$_2$ aqueous solution (see Fig. 1). The length of the BN nanotubes was 15 Å and the radius was 4.89 Å and 5.54 Å for the (7,7) and (8,8) chirality nanotubes, respectively. The BN nanotubes and the membrane affect each other via both van der Waals and electrostatic interactions. Due to the partial charges on the boron and nitrogen atoms of BN nanotubes and silicon and nitrogen atoms of silicon-nitride membrane, electrostatic interactions are dominant and the source of selectivity for ion transport.

Methods

We used BN nanotubes with (7,7) and (8,8) chirality and optimized their geometries at the B3LYP level of theory using the 6–31G(2d,2p) basis set, accomplished in the GAMESS-US package [36]. The optimized B-N bond distance was calculated as 1.446 Å. Partial charges used in the MD simulation were −0.4 and +0.4 for nitrogen and boron atoms, respectively. In addition, the length of the BN nanotubes in their selectivity properties had no effect. For B and N atoms, the Lennard-Jones parameters were obtained from Aluru [37, 32], with the following parameters: ε_{boron}=0.094 kcal mol^{-1}, σ_{boron}=3.453 Å, $\varepsilon_{nitrogen}$=0.144 kcal mol^{-1}, and $\sigma_{nitrogen}$=3.365 Å. The interaction parameters between different species systems were obtained using Lorentz-Berthelot combining rules. In this work, we used the partial charges determined by DFT for BN nanotubes [38].

We performed molecular dynamics simulations using Nanoscale Molecular Dynamics program (NAMD) [39] as in previous works [40, 41] with a 1 fs time step and visualized using visual molecular dynamics (VMD) [42]. In the NAMD package, the potential energy of intermolecular interactions is given through Eq. 1.

$$U_{(r_{ij})} = 4\,\varepsilon_{ij}\left[\left(\frac{\sigma_{ij}}{r_{ij}}\right)^{12} - \left(\left(\frac{\sigma_{ij}}{r_{ij}}\right)\right)^{6}\right] + \frac{q_i.q_j}{4\pi\varepsilon_0 r_{ij}}, \qquad (1)$$

where r_{ij} is the distance between the atoms i and j, q_i and q_j are the partial charge assigned to atoms i and j, and ε_{ij} and σ_{ij} are the usual empirical Lennard-Jones parameters, obtained by Lorentz-Berthelot combining rules, where $\sigma_{ij}=(\sigma_i+\sigma_j)/2$ and $\varepsilon_{ij}=(\varepsilon_{ij}.\varepsilon_{ij})^{0.5}$. Also, all analysis scripts were composed locally
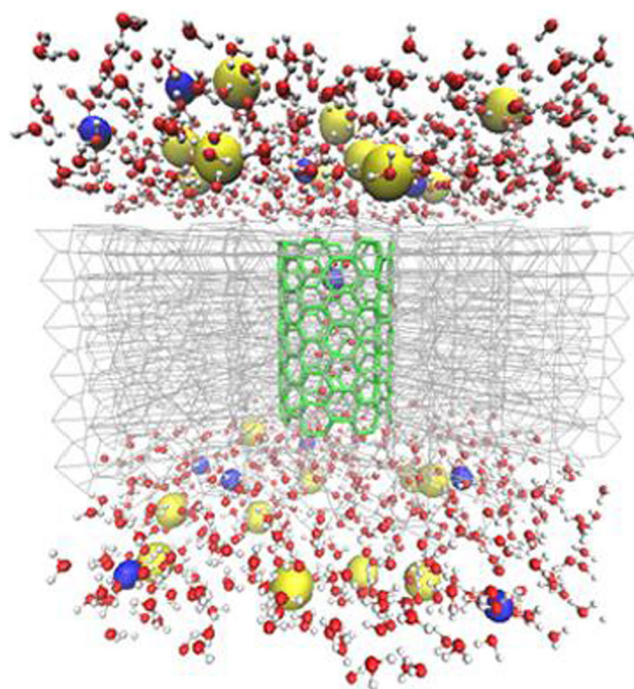

Fig. 1 A snapshot of the simulated system (*green*: (7,7) BN nanotube, tan: silicon-nitride membrane, *blue*: Zn^{2+}; *yellow*: Cl$^-$; *red*: O; *white*: H)

using the VMD and Tcl commands. The simulation settings are as follows: (*i*) van der Waals interactions were truncated by a 12 Å cutoff, (*ii*) the particle mesh Ewald algorithm [43] was used for electrostatic calculations with an interpolation function of order 5, (*iii*) the MD domain consisted of a BN nanotube, a silicon-nitride membrane, water, and ions, (*iv*) the periodic boundary conditions were used in all three directions to mimic systems with an infinitely large area, (*v*) the simulation box for all runs was 35×41×50 Å^3, and (*vi*) the system was subjected to a zero-temperature energy minimization for 0.5 ns and then equilibrated with molecular dynamics for 5 ns at 298 K before data collection.

An electric field was used for all of the systems in the simulation. The applied electric field was defined by Eq. 2.

$$e_{field} = -23.0605492\frac{V}{l_z}, \qquad (2)$$

where e_{field}, V, and l_z are the applied electric field (in kcal (mol Å e)$^{-1}$), potential difference (in volts), and size of the system along the z-axis (in Ångstroms), respectively [44]. The structure was equilibrated for 0.5 ns to a constant pressure of 1 bar and a constant temperature of 298 K. We employed the Langevin dynamics method to keep the temperature at 298 K. The pressure was maintained at 1 bar using a Nose-Hoover Langevin piston. To represent water molecules, the TIP3P model (the intermolecular three-point potential) was used [45]. This model is remarkably successful at modeling liquid water under ambient conditions and is reasonably successful under other conditions. Three site models have three

interaction points corresponding to the three atoms of the water molecule. Each site has a point charge, and the site corresponding to the oxygen atom also has the Lennard-Jones parameters. Since 3-site models achieve a high computational efficiency, these are widely used in molecular dynamics simulations. Most of the models use a rigid geometry matching that of actual water molecules. One of these models is the TIP3P model, which assumes an ideal shape (HOH angle of 104.52°) and partial charge for hydrogen and oxygen atoms are +0.417 and −0.834, respectively. The CHARMM force field [46] was employed to describe the interatomic interactions for all atoms. In this work, the silicon-nitride membrane and the BN nanotubes were restrained with a harmonic constraint for all runs, while water molecules and ions were allowed to move freely. The current versus voltage curve for the studied systems was obtained at an ionic concentration of 0.5 mol L^{-1}. The amount of current was calculated by Eq. 3.

$$I = n.q/\Delta t, \tag{3}$$

where n, q, and Δt are the average number of ions that cross the BN nanotube, the charge of the ion, and the simulation time of one run, respectively.

The contrasting ion selectivity of BN nanotubes was illustrated by calculating the potential of mean force (PMF) [47] along the z-axis. After averaging the force on the molecules at different z positions along the nanotube axis, PMF was calculated by means of integrating the mean force along the z-axis. The ends of the reservoirs were taken as the reference position where the PMF was zero.

The ion was moved through positions from 0 to 15 Å in 0.5 Å increments. The z component of ions was held using a harmonic constraint of 12.5 kcal mol^{-1} $Å^{-2}$ while the ion was free to move radially. This harmonic constraint was selected to give enough overlap between each window and its neighbors while constraining the ions enough to ensure adequate sampling of the entire reaction coordinate. Each sampling window is run for 1 ns. The PMF of the ion moving through the nanotube was computed by the umbrella sampling technique [48] and the data were analyzed using the weighted histogram analysis method (WHAM) [49].

Results and discussion

We performed molecular dynamics simulations to investigate the separation of Zn^{2+} ions from water through BN nanotubes with different chirality. Additionally, to study other properties of the system, the following parameters were obtained: the ionic current, normalized transport rate of water, retention time and ion-water radial distribution functions.

Water is a good solvent for ions and polar molecules and an exceptionally poor solvent for non-polar or hydrophobic solutes [50, 51]. The interaction of ions with water can lead to breakage of this structure, replaced by a different order of the molecules in the local field of the ion. Figure 2 shows the organization of water molecules in BN nanotubes. In Fig. 2a, the dipole vector of the water molecules orients to the walls of (7,7) BN nanotube, while in Fig. 2b, the dipole vector of the water molecules orients toward the axis of (8,8) BN nanotube. In fact, their orientation is in such a way that in the (7,7) BN nanotube, and zinc atoms (with a positive charge) are near the oxygen atoms (with a negative charge). In the (8,8) BN nanotube chlorine atoms (with a negatively charge) are near the hydrogen atoms (with a positive charge). The orientation of dipole vector of water molecules was due to different atoms that were located in the surrounding BN nanotubes. The nitrogen and silicon atoms of the membrane were surrounded in the (7,7) BN nanotube and (8,8) BN nanotube, respectively, as shown in Fig. 3. These arrangements of atoms depend on the size of the embedded pore. According to DFT calculations, the nitrogen atoms of the BN nanotubes shift outward due to the electronic structure. With a (7,7) BN nanotube embedded in a silicon-nitride membrane, nitrogen atoms in the matrix surround the outer surface of the pore, thus causing the boron atoms of the tube to shift slightly outward relative to the nitrogen atoms of the tube. Conversely, with the (8,8) BN nanotube, silicon atoms surround the surface of the pore, and the nitrogen atoms of the nanotube move outward relative to the boron atoms. Small shifts in the relative positions of the boron and nitrogen atoms partially account for the ion selectivity observed in our system.

Although the considered BN nanotubes had a large radius to accept cations and anions, our results indicate that one Zn^{2+} ion entered the (7,7) BN nanotube, and was able to come out. In contrast, chlorine ions could not enter the (7,7) BN nanotube. In the case of the (8,8) BN nanotube, the opposite phenomenon occurred. This different behavior was governed by the different orientation of the dipole vector of the water molecules (see Fig. 2).

Since the ionic radius of chlorine is greater than zinc, the Zn^{2+} ions with smaller ionic radii are able to pass through the (7,7) BN nanotube. However, this different ionic radius is not the main reason for the selective passage of ions from BN nanotubes but it can be an auxiliary factor. As mentioned above, the main cause of this phenomenon is the different orientation of the dipole vector of the water molecules.

The most important observation seems to be that the nature of the BN nanotubes has a large effect in determining the ion-specific flux and is more important than the nature of the embedding membrane. Specifically, Zn^{2+} ions encountered a favorable PMF in entering (7,7) BN nanotube, while the Cl^- ions are repelled from it. In the case of (8,8) BN nanotube showed different behavior than (7,7) BN nanotube. The (8,8)
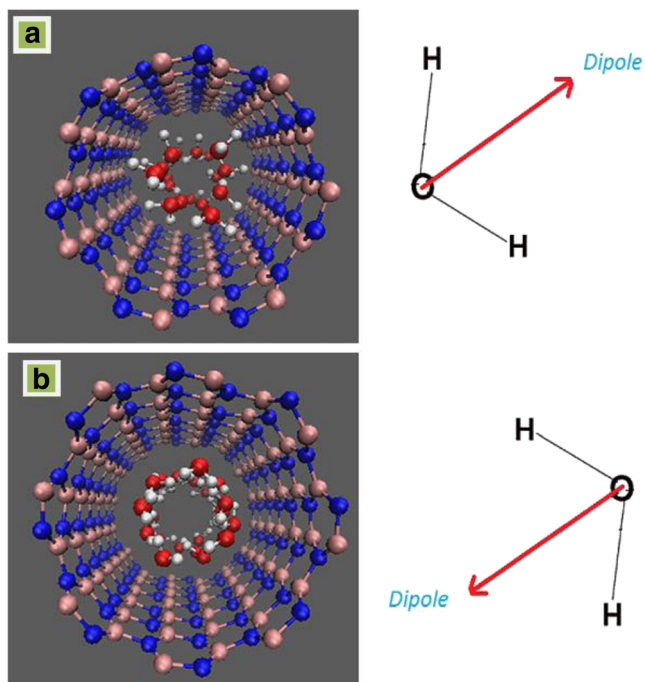
Fig. 2 The orientation of water molecules within BN nanotubes: **a**: (7,7) BN nanotube; **b**: (8,8) BN nanotube

Fig. 4 The potential of mean force for Zn^{2+} and Cl^- ions in **a**: (7,7) BN nanotube ; **b**: (8,8) BN nanotube

BN nanotube was favorable for Cl^- ions permeation, while the Zn^{2+} ions are repelled from it.

The thermodynamic basis of the observed ion selectivity was explored by the calculation of potentials of mean force for a given ion as it moved along the (z) axis of the pore. Figure 4 shows the PMF values for the studied systems. Figure 4a shows that in the case of (7,7) BN nanotube, there was an energy barrier for chloride ions to prevent them from entering into the (7,7) BN nanotube.

In the case of (8,8) BN nanotube, an energy barrier exists for Zn^{2+} ions, as shown in Fig. 4b. In these BN nanotubes, a deep energy well for ions occurred due to dipole of the water molecules inside the nanotube. The PMF was computed without any external field. When no electric field was applied, the ions could enter the BN nanotube and accumulated near the
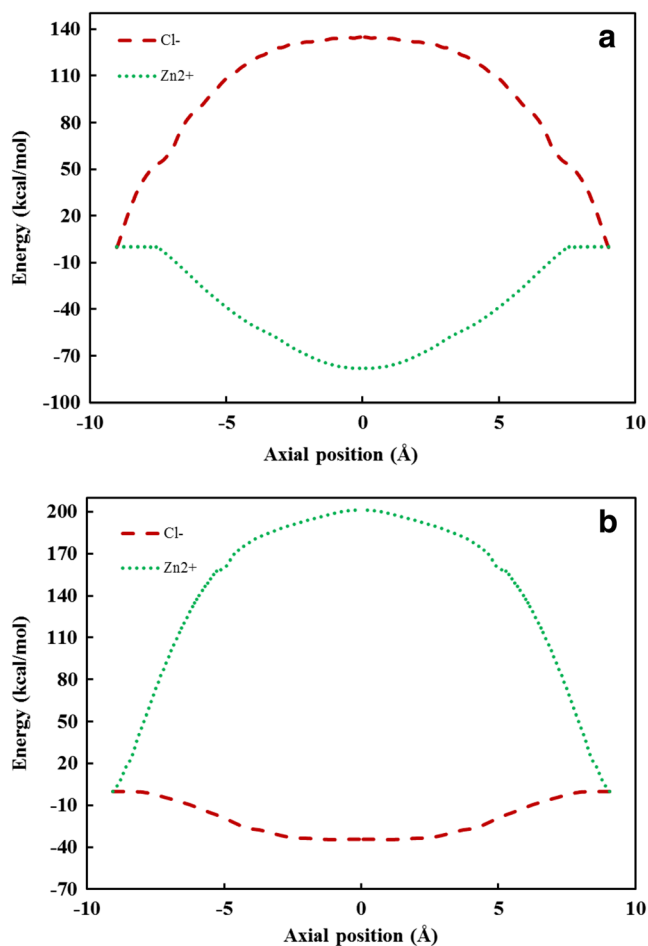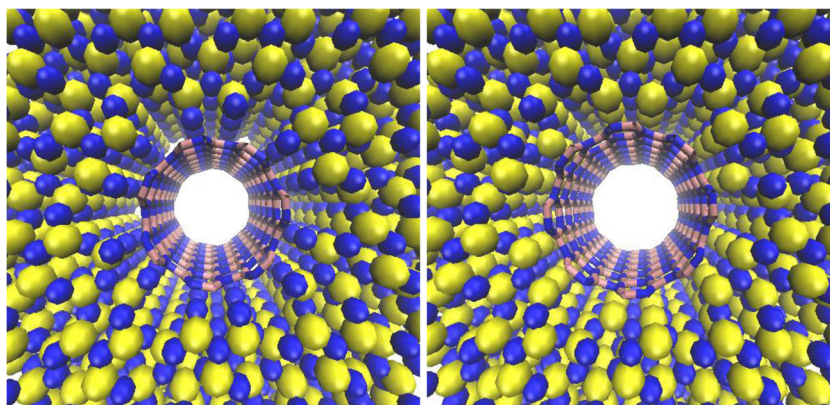
pore center. In the case of application of an electric field, the ions overcame the potential barrier and could exit from the nanotube.

In our simulations, the PMF was increased at the pore openings and reached a maximum value at the pore center inside the BN nanotube. This was due to the high symmetry of the system and interactions between anions, BN nanotubes, and the membrane. This is in agreement with the results of

Fig. 3 Left: Nitrogen atoms of the membrane surrounding a (7,7) BN nanotube. Right: Silicon atoms of the membrane surrounding an (8,8) BN nanotube (blue and cyan: BN nanotube; blue: nitrogen atoms of the membrane; yellow: silicon atoms of the membrane)
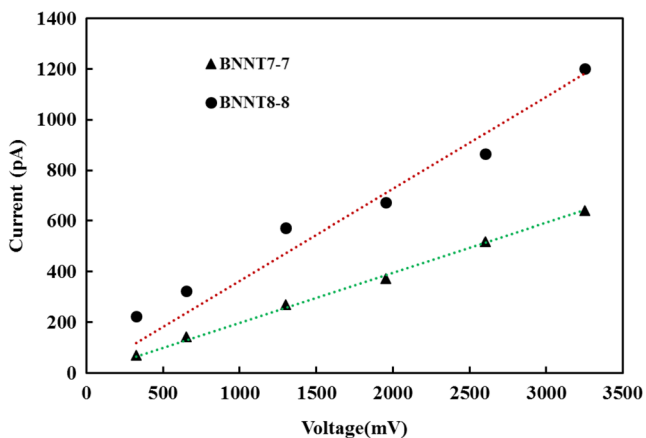
Fig. 5 Current–voltage curves for Zn^{2+} ions in (7,7) BN nanotube and Cl^- ion in (8,8) BN nanotube. Each data point represents the average of five sets of simulations. Lines were obtained from linear regression

simulations showing that anions cannot penetrate the (7,7) BN nanotube because PMF has a high free energy barrier [52, 53].

Figure 5 presents the current–voltage profile obtained by Eq. 3. The current was increased linearly by increasing the voltage. The linear increase in the current with rising voltage
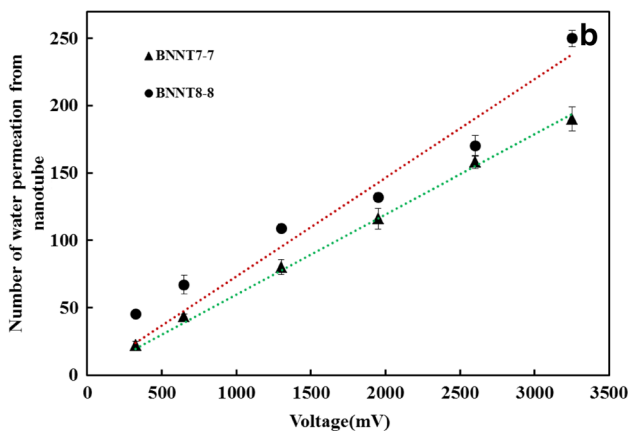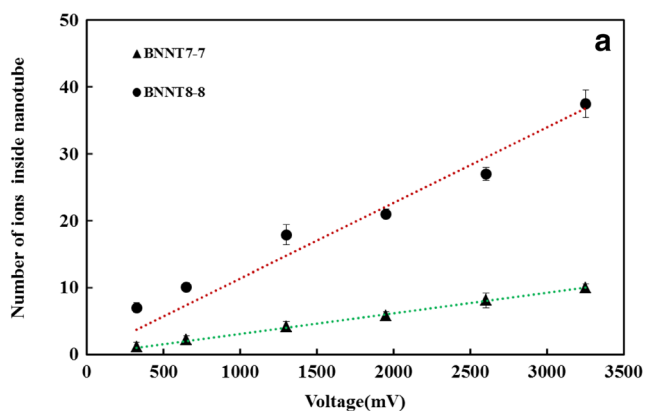

Fig. 6 a: The number of ions passing through a BN nanotube: Zn^{2+} ions in (7,7) BN nanotube and Cl^- ions in (8,8) BN nanotube. **b**: The number of water molecules passing through the BN nanotubes. Error bars represent one standard error of the mean and error bars smaller than the data points are not shown

Table 1 Transport rate for water molecules

Electric field	Transport rate	
(mV)	(7,7) BN nanotube	(8,8) BN nanotube
325.23	4.4	9
650.46	8.6	13.4
1300.92	16	21.8
1951.38	23.2	26.4
2601.84	31.6	34
3252.3	38	50

indicated that the number of ions and water molecules passing across the (7,7) and (8,8) BN nanotubes increased linearly with applied voltage (Fig. 6). By fitting a linear regression model to the current–voltage curve, we obtained zinc and chloride conductance values of 363.7 picosiemens (pS) and 197.8 pS for the (7,7) and (8,8) BN nanotubes, respectively.

We computed the transport rate of the water molecules as the ratio of the average number of water molecules passing across the (7,7) and (8,8) BN nanotubes according to the simulation time (see Table 1). As seen in Table 1, the transport rate of water increased with increasing voltage. Also, this parameter was larger for the (8,8) BN nanotube than for (7,7) BN nanotube due to the large diameter of (8,8) BN nanotube.

Another simulation parameter studied in this work was the normalized transport rate of water with respect to the number of transported ions (see Fig. 7). These results show that the value of this parameter does not change by changing the voltage and so is independent of the voltage. Also, this parameter was greater for (7,7) BN nanotube than (8,8) BN nanotube. The reason is that although the number of ions passing through the (7,7) BN nanotube were lower than the
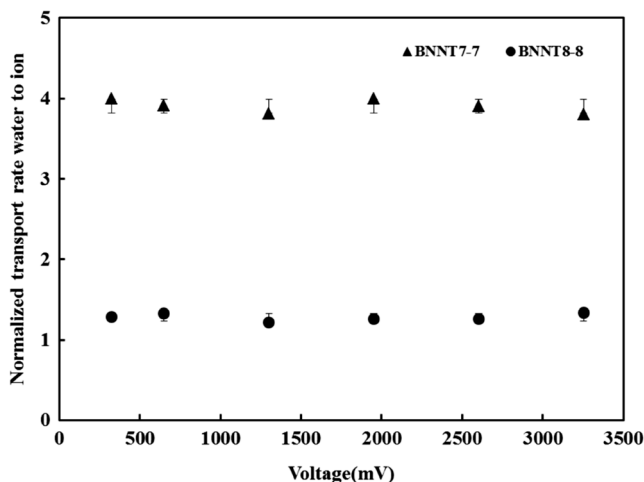

Fig. 7 Normalized transport rate of water molecules to ions. Error bars represent one standard error of the mean and error bars smaller than the data points are not shown
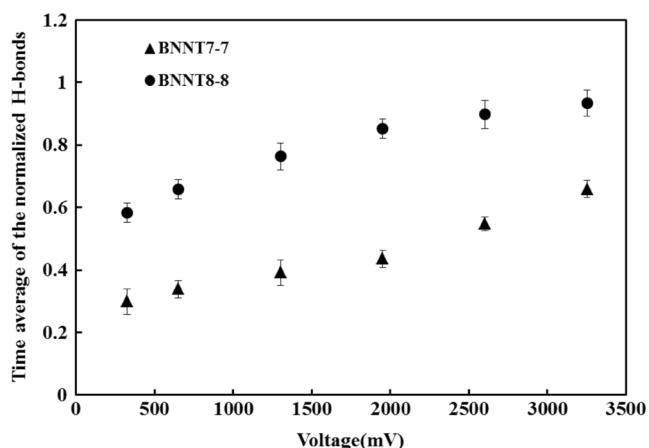
Fig. 8 The time average of the normalized H-bonds. Error bars represent one standard error of the mean and error bars smaller than the data points are not shown

(8,8) BN nanotube, the hydration number of Zn^{2+} ion was larger than the hydration number of Cl^- ion (see Fig. 11). In Fig. 11, the peak intensity of the radial distribution function of Zn^{2+}-water in the (7,7) BN nanotube was more than that of Cl^--water in the (8,8) BN nanotube.

The water network structure inside the BN nanotubes was interrupted by the construction of the first hydration shell around the ion. This caused a reduction in the number of hydrogen bonds between water molecules [54, 55]. To investigate this phenomenon, we computed the time average of the normalized hydrogen bonds with respect to the number of inner water molecules at different voltages (see Fig. 8). As expected, this parameter increased with increasing voltage. The time average of the normalized hydrogen bonds was greater for (8,8) BN nanotube than (7,7) BN nanotube. In addition, Fig. 9 shows the water density inside the BN nanotubes over 5 ns. In this figure, the density of water increased with increasing voltage due to the high transport of ions at

high voltage. Also, due to the large diameter of (8,8) BN nanotube, the water density was higher than that in (7,7) BN nanotube.

Figure 10 indicates the retention time of the ions, which is the time passage of one ion through the (7,7) and (8,8) BN

Fig. 10 Retention time for ions at applied voltages: Zn^{2+} in (7,7) BN nanotube and Cl^- in (8,8) BN nanotube
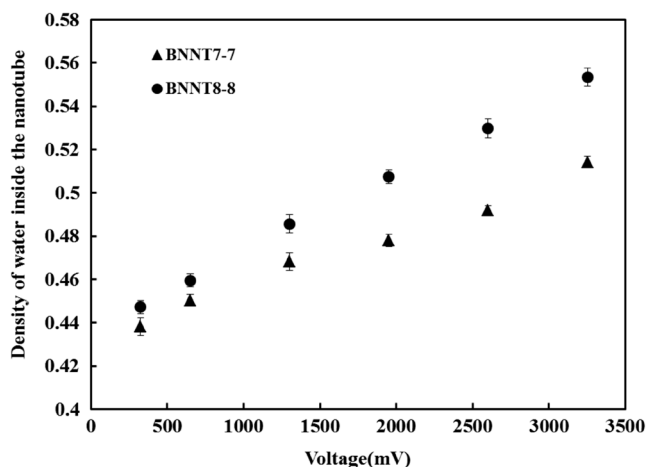

Fig. 9 Density of water inside the BN nanotubes. Error bars represent one standard error of the mean and error bars smaller than the data points are not shown
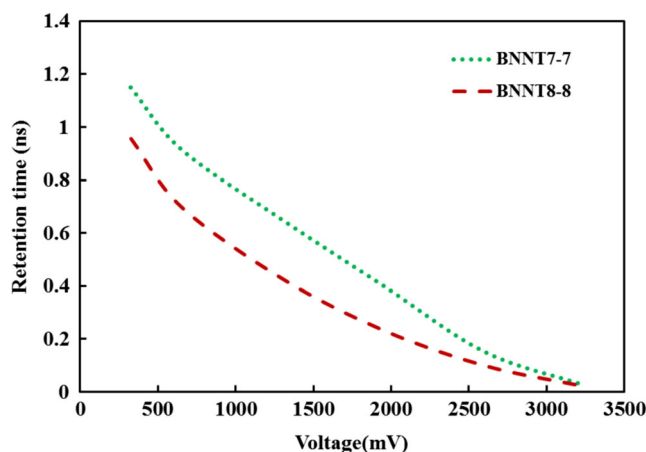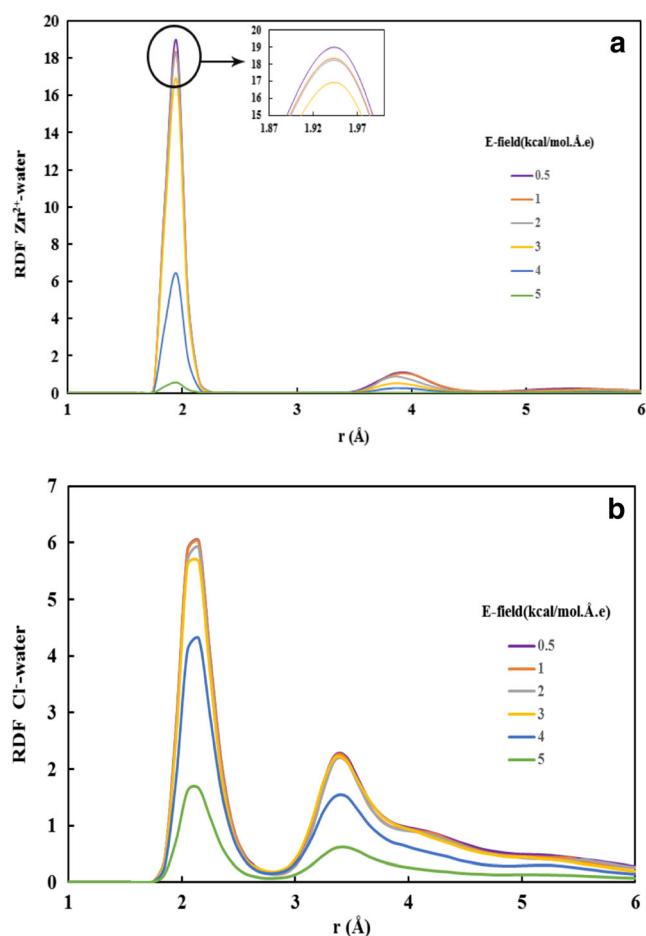
Fig. 11 Ion-water radial distribution function within the BN nanotubes under various electric fields: **a**: (7,7) BN nanotube and **b**: (8,8) BN nanotube

nanotubes as a function of applied voltage. This figure shows that a short retention time was found with a strong electric field. The retention time for Zn^{2+} in the (7,7) BN nanotube was higher than that of Cl^- in the (8,8) BN nanotube. As seen in Fig. 4, in the case of (7,7) BN nanotube, there was an energy well for zinc ions inside the nanotube that is deeper than the energy well for chloride ions in the (8,8) BN nanotube. As a result, due to the deep energy well of zinc ions in the (7,7) BN nanotube, they spend more time within the nanotube which increases the retention time of zinc ions. However, because of the small energy well of the chloride ion in the (8,8) BN nanotube, Cl^- passes through the nanotube easily, which caused the short retention time. These factors and their effects on the current were also shown in Fig. 5, so that the current through the (8,8) BN nanotube was higher than through the (7,7) BN nanotube (see Fig. 5). Due to this, in the case of the (8,8) BN nanotube, the retention time was short. This phenomenon shows itself in the radial distribution function. As can be seen, the intensity peak of the radial distribution

function of the (8,8) BN nanotube was less than that of the (7,7) BN nanotube.

To describe the structural change of each type of molecule/atom in the simulation cell, the radial distribution function (RDF) was calculated from the trajectories saved during the simulation. Figure 11 illustrates the RDF between ions and water molecules. As can be seen at a short distance, because of the repulsive forces between species, RDF is zero. The position of the first maximum and minimum peak is the same in all cases. Nevertheless, the location of the tip of the peak is different in each case, which indicates that the number of water molecules in the first hydration shell of the ion is different [53]. Figure 11a shows the Zn^{2+}-water RDF inside (7,7) BN nanotube, while Fig. 11b shows the Cl^--water RDF inside (8,8) BN nanotube. Also, it can be seen that the RDFs varied with changing the electric field. These variations can be explained based on retention times of the ions. At low voltages, ions spend more time in BN nanotubes within the hydration shell. In other words, they have a long retention time and therefore the RDF would be intensified. Figures 10 and 11 indicate that the order of RDFs and retention times for the ions are the same. The RDF with a high peak corresponds to a long retention time or weak electric field.
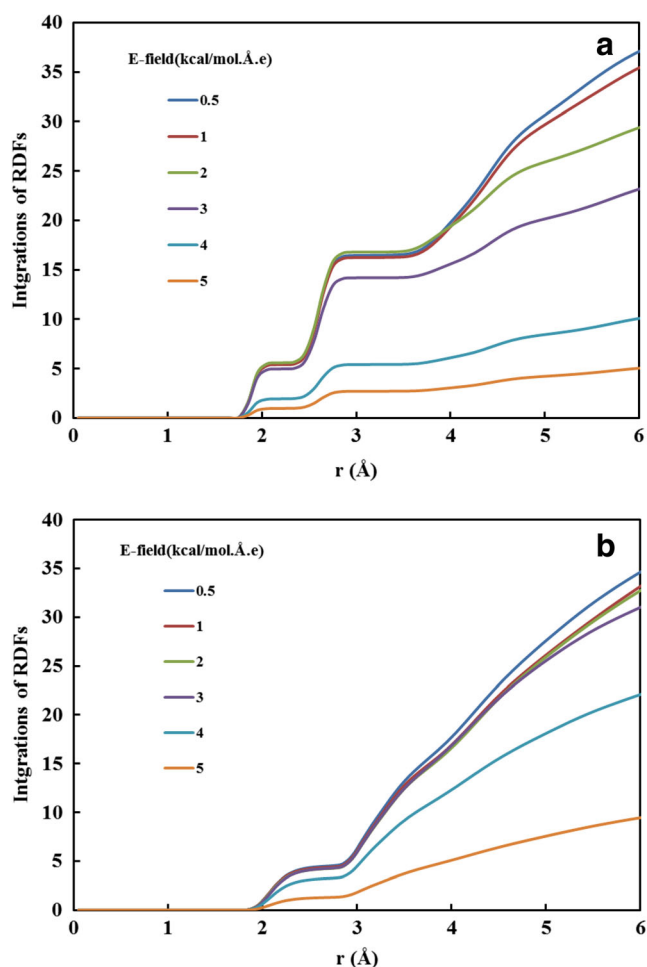

Fig. 12 Hydration number of the considered ions within the BN nanotubes under various electric fields: **a**: (7,7) BN nanotube and **b**: (8,8) BN nanotube
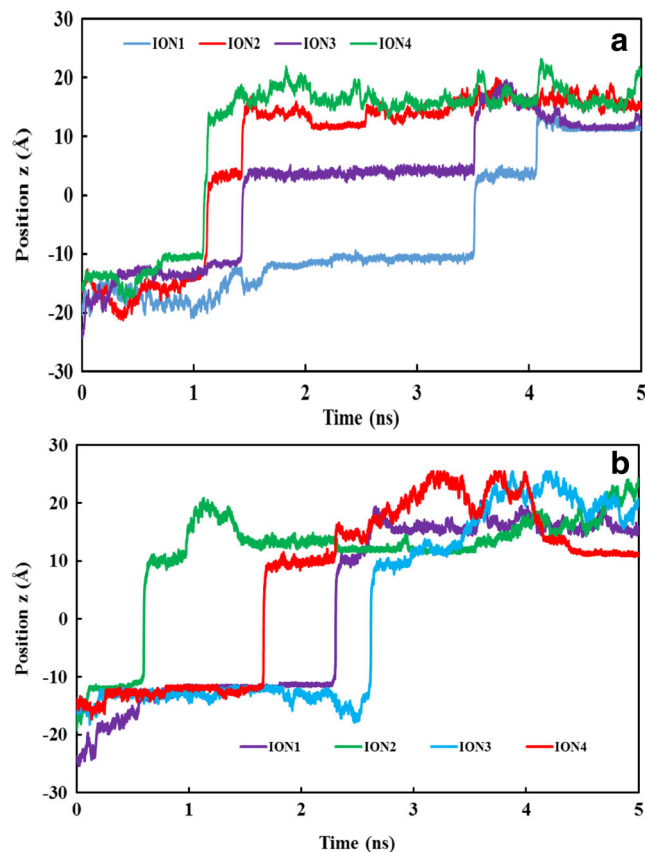

Fig. 13 The z positions of the ions for each simulation at **a**: low voltage and **b**: high voltage

Figure 12 also includes a graph of the integral of ions-water RDF that is equal to the hydration number of the considered ions. This integral is calculated by Eq. 4

$$N_{ij} = 4\pi \int_0^r \rho.g_{(r)}.r^2.dr, \qquad (4)$$

in which N_{ij}, ρ, $g_{(r)}$, and r are the number of i molecules around molecule j, density, radial distribution function and the radial coordinate respectively.

Figure 13 displays the z positions of the ions inside the BN nanotubes. As can be seen, an overlap exists between the retention times of ions at low voltages. On the other hand, for high voltages, this overlap does not exist. This implies that, with a weak electric field, an ion can go into the BN nanotube and after entry of the second ion, cannot exit. However, in a strong electric field, ions can exit the BN nanotube without any help [56].

Conclusions

Molecular dynamics simulations method were used to study the permeability of nanotubes for ion selectivity through (7,7) and (8,8) BN nanotubes. The ion permeation through an armchair BN nanotube fixed in a silicon-nitride membrane was selective in the presence of electric field. When a Zn^{2+} ion entered the (7,7) BN nanotube, it was able to pass the entire length of the nanotube and it came out; Cl^- ions were not able to enter the (7,7) nanotube. In the case of the (8,8) BN nanotube, the opposite phenomenon occurred. In (7,7) and (8,8) BN nanotubes, the preferential permeation was reached without functionalizing the BN nanotubes. The simplicity of the structure is an advantage for the fabrication nanodevice for the separation of heavy metals. It can be concluded that the application of electric field can have an impact on the following properties of the studied systems: PMF, the ionic current, ion retention time, water density, transport rate of the water molecules, and RDF.

References

1. Stafiej A, Pyrzynska K (2007) Adsorption of heavy metal ions with carbon nanotubes. Sep Purif Technol 58(1):49–52. doi:10.1016/j.seppur.2007.07.008
2. Hsieh S-H, Horng J-J (2007) Adsorption behavior of heavy metal ions by carbon nanotubes grown on microsized Al_2O_3 particles. J Univ Sci Technol Beijing 14(1):77–84. doi:10.1016/S1005-8850(07)60016-4
3. Gao J, Sun S-P, Zhu W-P, Chung T-S (2014) Polyethyleneimine (PEI) cross-linked P84 nanofiltration (NF) hollow fiber membranes for Pb^{2+} removal. J Membr Sci 452(0):300–310. doi:10.1016/j.memsci.2013.10.036
4. Han KN, Yu BY, Kwak S-Y (2012) Hyperbranched poly (amido-amine)/polysulfone composite membranes for Cd (II) removal from water. J Membr Sci 396(0):83–91. doi:10.1016/j.memsci.2011.12.048
5. Wang R, Guan S, Sato A, Wang X, Wang Z, Yang R, Hsiao BS, Chu B (2013) Nanofibrous microfiltration membranes capable of removing bacteria, viruses and heavy metal ions. J Membr Sci 446(0):376–382. doi:10.1016/j.memsci.2013.06.020
6. Yoo H, Kwak S-Y (2013) Surface functionalization of PTFE membranes with hyperbranched poly (amidoamine) for the removal of Cu^{2+} ions from aqueous solution. J Membr Sci 448(0):125–134. doi:10.1016/j.memsci.2013.07.052
7. Zhang L, Zhao Y-H, Bai R (2011) Development of a multifunctional membrane for chromatic warning and enhanced adsorptive removal of heavy metal ions: application to cadmium. J Membr Sci 379(1–2):69–79. doi:10.1016/j.memsci.2011.05.044
8. Huang K, Xiu Y, Zhu H (2013) Removal of heavy metal ions from aqueous solution by chemically modified mangosteen pericarp. Desalin Water Treat 51:1–9. doi:10.1080/19443994.2013.838522
9. Oyaro N, Juddy O, Murago EN, Gitonga E (2007) The contents of Pb, Cu, Zn and Cd in meat in nairobi, Kenya. Kenya Int J Food Agric Environ 5:119–121
10. Alyüz B, Veli S (2009) Kinetics and equilibrium studies for the removal of nickel and zinc from aqueous solutions by ion exchange resins. J Hazard Mater 167(1–3):482–488. doi:10.1016/j.jhazmat.2009.01.006
11. El Samrani AG, Lartiges BS, Villiéras F (2008) Chemical coagulation of combined sewer overflow: heavy metal removal and treatment optimization. Water Res 42(4–5):951–960. doi:10.1016/j.watres.2007.09.009
12. Ghosh P, Samanta AN, Ray S (2011) Reduction of COD and removal of Zn^{2+} from rayon industry wastewater by combined electro-fenton treatment and chemical precipitation. Desalination 266(1–3):213–217. doi:10.1016/j.desal.2010.08.029
13. Cséfalvay E, Pauer V, Mizsey P (2009) Recovery of copper from process waters by nanofiltration and reverse osmosis. Desalination 240(1–3):132–142. doi:10.1016/j.desal.2007.11.070
14. Yanagisawa H, Matsumoto Y, Machida M (2010) Adsorption of Zn (II) and Cd (II) ions onto magnesium and activated carbon composite in aqueous solution. Appl Surf Sci 256(6):1619–1623. doi:10.1016/j.apsusc.2009.10.010
15. Alidokht L, Khataee AR, Reyhanitabar A, Oustan S (2011) Cr (VI) immobilization process in a Cr-spiked soil by zerovalent iron nanoparticles: optimization using response surface methodology. Clean 39(7):633–640. doi:10.1002/clen.201000461
16. Alidokht L, Khataee AR, Reyhanitabar A, Oustan S (2011) Reductive removal of Cr (VI) by starch-stabilized Fe^0 nanoparticles in aqueous solution. Desalination 270(1–3):105–110. doi:10.1016/j.desal.2010.11.028
17. Khataee AR, Kasiri MB, Alidokht L (2011) Application of response surface methodology in the optimization of photocatalytic removal of environmental pollutants using nanocatalysts. Environ Technol 32(15):1669–1684. doi:10.1080/09593330.2011.597432
18. Reyhanitabar A, Alidokht L, Khataee AR, Oustan S (2012) Application of stabilized Fe0 nanoparticles for remediation of Cr (VI)-spiked soil. Eur J Soil Sci 63(5):724–732. doi:10.1111/j.1365-2389.2012.01447.x
19. Golberg D, Bando Y, Tang CC, Zhi CY (2007) Boron nitride nanotubes. Adv Mater 19(18):2413–2432. doi:10.1002/adma.200700179
20. Anota EC, Cocoletzi G, Ramírez JFS (2013) Armchair BN nanotubes—levothyroxine interactions: a molecular study. J Mol Model 19(11):4991–4996. doi:10.1007/s00894-013-1999-1

21. Chigo Anota E, Cocoletzi G (2013) First-principles simulations of the chemical functionalization of (5,5) boron nitride nanotubes. J Mol Model 19(6):2335–2341. doi:10.1007/s00894-013-1782-3

22. Won CY, Aluru NR (2009) A chloride ion-selective boron nitride nanotube. Chem Phys Lett 478(4–6):185–190. doi:10.1016/j.cplett.2009.07.064

23. Chen X, Wu P, Rousseas M, Okawa D, Gartner Z, Zettl A, Bertozzi CR (2009) Boron nitride nanotubes are noncytotoxic and can be functionalized for interaction with proteins and cells. J Am Chem Soc 131(3):890–891. doi:10.1021/ja807334b

24. Nanok T, Artrith N, Pantu P, Bopp PA, Limtrakul J (2008) Structure and dynamics of water confined in single-wall nanotubes. J Phys Chem A 113(10):2103–2108. doi:10.1021/jp8088676

25. Akdim B, Pachter R, Duan X, Adams WW (2003) Comparative theoretical study of single-wall carbon and boron-nitride nanotubes. Phys Rev B Condens Matter 67(24):245404

26. Rubio A, Corkill JL, Cohen ML (1994) Theory of graphitic boron nitride nanotubes. Phys Rev B Condens Matter 49(7):5081–5084

27. Chopra NG, Luyken RJ, Cherrey K, Crespi VH, Cohen ML, Louie SG, Zettl A (1995) Boron nitride nanotubes. Science 269(5226):966–967. doi:10.1126/science.269.5226.966

28. Golberg D, Bando Y, Eremets M, Takemura K, Kurashima K, Yusa H (1996) Nanotubes in boron nitride laser heated at high pressure. Appl Phys Lett 69(14):2045–2047. doi:10.1063/1.116874

29. Lourie OR, Jones CR, Bartlett BM, Gibbons PC, Ruoff RS, Buhro WE (2000) CVD growth of boron nitride nanotubes. Chem Mater 12(7):1808–1810. doi:10.1021/cm000157q

30. Chen Y, Willis JP (1999) Mechanochemical synthesis of boron nitride nanotubes. Mater Sci Forum 312:173–178

31. Han W, Bando Y, Kurashima K, Sato T (1998) Synthesis of boron nitride nanotubes from carbon nanotubes by a substitution reaction. Appl Phys Lett 73(21):3085–3087. doi:10.1063/1.122680

32. Won CY, Aluru NR (2008) Structure and dynamics of water confined in a boron nitride nanotube. J Phys Chem C 112(6):1812–1818. doi:10.1021/jp076747u

33. Ebro H, Kim YM, Kim JH (2013) Molecular dynamics simulations in membrane-based water treatment processes: A systematic overview. J Membr Sci 438:112–125. doi:10.1016/j.memsci.2013.03.027

34. Tang D, Kim D (2014) Temperature effect on ion selectivity of potassium and sodium ions in solution. Chem Phys 428:14–18. doi:10.1016/j.chemphys.2013.10.018

35. Khosrozadeh A, Wang Q, Varadan VK (2014) Molecular simulations on separation of atoms with carbon nanotubes in torsion. Comput Mater Sci 81:280–283. doi:10.1016/j.commatsci.2013.08.030

36. Schmidt MW, Baldridge KK, Boatz JA, Elbert ST, Gordon MS, Jensen JH, Koseki S, Matsunaga N, Nguyen KA, Su S, Windus TL, Dupuis M, Montgomery JA (1993) General atomic and molecular electronic structure system. J Comput Chem 14(11):1347–1363. doi:10.1002/jcc.540141112

37. Won CY, Aluru NR (2007) Water permeation through a subnanometer boron nitride nanotube. J Am Chem Soc 129(10):2748–2749. doi:10.1021/ja0687318

38. Sardroodi JJ, Azamat J, Rastkar A, Yousefnia NR (2012) The preferential permeation of ions across carbon and boron nitride nanotubes. Chem Phys 403:105–112. doi:10.1016/j.chemphys.2012.05.017

39. Kalé L, Skeel R, Bhandarkar M, Brunner R, Gursoy A, Krawetz N, Phillips J, Shinozaki A, Varadarajan K, Schulten K (1999) NAMD2: greater scalability for parallel molecular dynamics. J Comput Phys 151(1):283–312. doi:10.1006/jcph.1999.6201

40. Azamat J, Sardroodi J (2014) The permeation of potassium and chloride ions through nanotubes: a molecular simulation study. Monatsh Chem 145(6):881–890. doi:10.1007/s00706-013-1136-y

41. Azamat J, Khataee A, Joo SW (2014) Functionalized graphene as a nanostructured membrane for removal of copper and mercury from aqueous solution: a molecular dynamics simulation study. J Mol Graphics Modell 53:112–117. doi:10.1016/j.jmgm.2014.07.013

42. Humphrey W, Dalke A, Schulten K (1996) VMD: visual molecular dynamics. J Mol Graphics 14(1):33–308. doi:10.1016/0263-7855(96)00018-5

43. Darden T, York D, Pedersen L (1993) Particle mesh Ewald: an N·log(N) method for Ewald sums in large systems. J Chem Phys 98(12):10089–10092. doi:10.1063/1.464397

44. Phillips JC, Braun R, Wang W, Gumbart J, Tajkhorshid E, Villa E, Chipot C, Skeel RD, Kalé L, Schulten K (2005) Scalable molecular dynamics with NAMD. J Comput Chem 26(16):1781–1802. doi:10.1002/jcc.20289

45. Jorgensen WL, Chandrasekhar J, Madura JD, Impey RW, Klein ML (1983) Comparison of simple potential functions for simulating liquid water. J Chem Phys 79(2):926–935. doi:10.1063/1.445869

46. MacKerell AD, Bashford D, Bellott DRL, Evanseck JD, Field MJ, Fischer S, Gao J, Guo H, Ha S, Joseph-McCarthy D, Kuchnir L, Kuczera K, Lau FTK, Mattos C, Michnick S, Ngo T, Nguyen DT, Prodhom B, Reiher WE, Roux B, Schlenkrich M, Smith JC, Stote R, Straub J, Watanabe M, Wiórkiewicz-Kuczera J, Yin D, Karplus M (1998) All-atom empirical potential for molecular modeling and dynamics studies of proteins. J Phys Chem B 102(18):3586–3616. doi:10.1021/jp973084f

47. Kjellander R, Greberg H (1998) Mechanisms behind concentration profiles illustrated by charge and concentration distributions around ions in double layers. J Electroanal Chem 450(2):233–251. doi:10.1016/S0022-0728(97)00641-4

48. Torrie GM, Valleau JP (1977) Nonphysical sampling distributions in monte carlo free-energy estimation: umbrella sampling. J Comput Phys 23(2):187–199. doi:10.1016/0021-9991(77)90121-8

49. Grossfield A (2014) WHAM: the weighted histogram analysis method, version 2.0.8. http://membrane.urmc.rochester.edu/content/wham.

50. Heisenberg WK (1969) The structure and properties of water. Oxford University Press, Oxford

51. Franks F (1973) Water, a comprehensive treatise. Plenum, New York.

52. Hilder TA, Gordon D, Chung S-H (2009) Salt rejection and water transport through boron nitride nanotubes. Small 5(19):2183–2190. doi:10.1002/smll.200900349

53. Peter C, Hummer G (2005) Ion transport through membrane-spanning nanopores studied by molecular dynamics simulations and continuum electrostatics calculations. Biophys J 89(4):2222–2234. doi:10.1529/biophysj.105.065946

54. Lee SH, Rasaiah JC (2009) Local dynamics and structure of the solvated hydroxide ion in water. Mol Simul 36(1):69–73. doi:10.1080/08927020903115252

55. Hummer G, Rasaiah JC, Noworyta JP (2001) Water conduction through the hydrophobic channel of a carbon nanotube. Nature 414(6860):188–190

56. Kang JW, Byun KR, Lee JY, Kong SC, Choi YW, Hwang HJ (2004) Molecular dynamics study on the field effect ion transport in carbon nanotube. Phys E 24(3–4):349–354. doi:10.1016/j.physe.2004.06.040